AIAA 2002-0346
Simulations of Plasma Detachment in VASIMR

A.V. Ilin, F.R. Chang Díaz, J.P. Squire, A.G. Tarditi,
ASPL, JSC / NASA, Houston, TX,

B.N. Breizman,
UT, Austin, TX,

M.D. Carter,
ORNL, Oak Ridge, TN

40th AIAA Aerospace Sciences Meeting & Exhibit
14-17 January 2002 / Reno, NV

SIMULATION OF PLASMA DETACHMENT IN VASIMR

Andrew V. Ilin*, Franklin R. Chang Díaz†, Jared P. Squire‡, Alfonso G. Tarditi§,
Advanced Space Propulsion Laboratory, JSC / NASA, Houston, TX,
Boris N. Breizman¶, University of Texas at Austin, Austin, TX,
and Mark D. Carter#, Oak Ridge National Laboratory, Oak Ridge, TN

ABSTRACT

Detachment of the plasma exhaust is an essential element of a magnetic nozzle operation that requires experimental, analytic and computer simulation studies. The present work is devoted to computer simulations of the plasma detachment in the Variable Specific Impulse Magnetoplasma Rocket. Both particle simulation and MHD methods have been used and results are reported in this paper.

INTRODUCTION

A magnetic nozzle plays two important roles in the operations of the Variable Specific Impulse Magnetoplasma Rocket (VASIMR)[1,2,3,4]. First, the perpendicular spiral motion of ions is converted into the axial motion. Second, the plasma detaches from the thruster. Both effects are critical in providing rocket thrust. The goal of mathematical simulations, reported in the paper, is to help understand the physics of plasma detachment and to assist in the design of a thruster suitable for an actual flight test.

Computer simulations of plasmas are typically done by using one, or a combination of three general techniques: fluid models, numerical solution of kinetic equations (Vlasov / Fokker-Planck), and particle models.

Recent growth in computer speed and memory of has made the particle description particularly attractive[5]. Particle methods, both Particle-in-Cell (PIC) and direct simulation Monte-Carlo (DSMC) methods, have been effectively used for simulation of Pulsed Plasma Thrusters (PPT)[6], Hall Thrusters[7] as well as Ion Thrusters[8]. In this paper we describe a particle trajectory method[9], and compare it with other modeling techniques to provide a quite accurate description for VASIMR plasma exhaust. The particle code is used for demonstrating plasma detachment in VASIMR. The results of the particle code are compared with results of MHD codes and with analytical considerations.

PREVIOUS PLASMA DETACHMENT STUDIES

Previous studies of the plasma detachment in a magnetic nozzle used simple models for the plasma flow. Kosmahl's[10] and Sercel's[11] models involve calculation of trajectories of ions and electrons guiding centers for given vacuum magnetic field. They observe plasma detachment by analyzing how the ion velocities behave and how the ion trajectories cross magnetic field lines.

The study by Sercel showed the improvement of propulsive efficiency of the magnetic nozzle by introducing extra tuning electric coils, acting as magnetic lens. York's[12] and Hoopers's[13] model considers a single-fluid MHD flow for given magnetic field. The condition for detachment in Hooper's study is given by the scaling parameter $G < 2{,}750$, defined as $G = (eB_z r_p(z_0))^2 / (m_e m_i (2u(z_0))^2)$. This work continues the previous studies of plasma detachment in the magnetic nozzle by considering additional simulation methods to analyze the detachment.

MAGNETIC CONFIGURATION IN VASIMR

The VASIMR system consists of three major magnetic cells, denoted as "forward," "central," and "aft"[1,2,3,4]. A magnet configuration example (related to a 24 kW VASIMR thruster[14] conceptual design) and the corresponding magnetic field profile is shown in Figure 1.

The forward end-cell provides the injection of the neutral gas to be ionized by electromagnetic waves that are produced by helicon antenna. In the central-cell,

* Research Scientist, Muniz Engineering, Inc.
ilin@jsc.nasa.gov
† NASA Astronaut, ASPL Director
‡ Senior Research Scientist, Muniz Engineering, Inc.
§ Senior Research Scientist, SAIC
¶ Research Scientist, Institute for Fusion Studies
# Research Staff, Fusion Energy Division

the plasma is also electromagnetically heated by waves operating near the Ion-Cyclotron Resonant Frequency (ICRF). The aft end-cell ensures that the plasma will efficiently detach from the magnetic field to provide propulsion through a highly directed exhaust stream. This magnetic configuration allows the plasma exhaust to be guided and controlled over a wide range of plasma energies and densities.

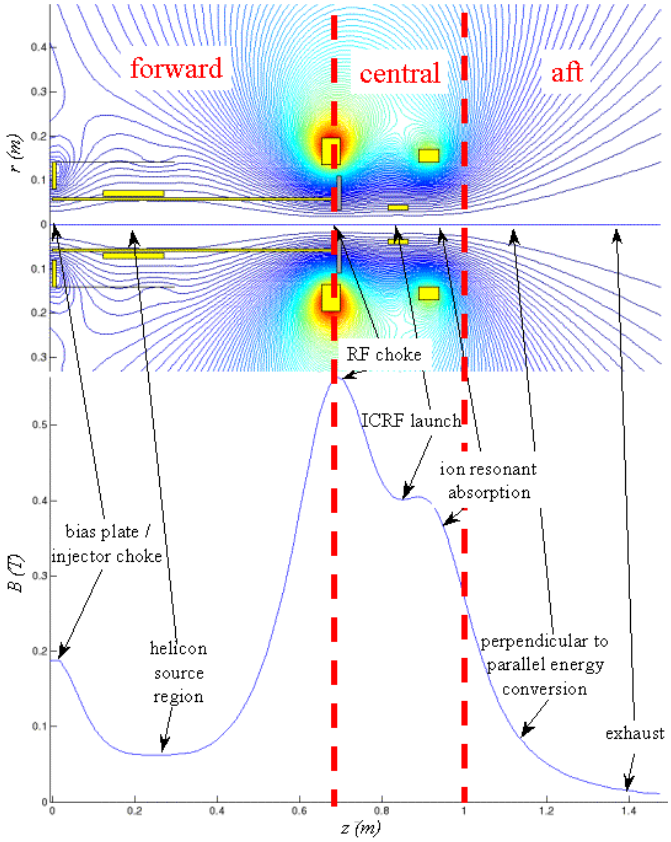

Figure 1: Geometry and magnetic field configuration for 24 kW VASIMR thruster.

In Figure 1, the forward end-cell is located at $z < 0.7$ *(m)*, the central cell at $0.7 < z < 1$ and the aft end-cell is at $1 < z$. In this paper we investigate the plasma exhaust in the aft end-cell in the domain $1 < z < 5$. The position $z_0 = 1$ *(m)* will be referred as the inlet of the exhaust.

Currently, the VASIMR system is under development for a first space flight experiment using *24 kW* of DC electric power. In the future, several megawatt VASIMR thrusters will be considered for human interplanetary flights to Mars and beyond[15]. This paper deals with exhaust plasma detachment for the *24 kW* VASIMR thruster (VF-24), which is assumed to have the operational parameters shown in Table 1.

	Operating parameter	**Definition/Typical value**
1.	Input power	$P = 24{,}000$ *(W)*
2.	Power efficiency (fraction of the input power going into the thrust power).	$e = 0.4$
3.	Specific impulse	$I_{sp} = 10{,}000$ *(sec).*
4.	Exhaust thrust velocity	$u = I_{sp} g = 10^5$ *(m/s)*
5.	Thrust force	$F = \frac{2eP}{u} = 0.192$ *(N).*
6.	Propellant rate	$\dot{m} = \frac{F}{u} = 1.92 \cdot 10^{-6}$ *(kg/s).*
7.	Propellant ion mass in terms of proton mass	$m_i = 2\, m_p$ (Deuterium)
8.	Exhaust ion energy	$W_i = \frac{m_i u^2}{2e} = 100$ *(eV)*
9.	Radius of plasma at the exhaust inlet	$r_p(z_0) = 0.05$ *(m)*
10.	Directed energy of the plume at the exhaust inlet	$W_z(z_0) = \frac{1}{2} W_i = 50$ *(eV)*
11.	Electron temperature is assumed constant	$T_e = 5$ *(eV)*
12.	Orthogonal ion temperature at the exhaust inlet	$T_{i\wedge} = \frac{1}{2} W_i = 50$ *(eV)*
13.	Average ion density at the exhaust inlet	$\bar{n}_i = \frac{\dot{m}}{m_i \pi r_p(z_0)^2 v_{\|\|}(z_0)} = 10^{18}\ (m^{-3})$
14.	Maximum ion density at the exhaust inlet	$n_{max} = 2\, \bar{n}_i = 2\, 10^{18}\ (m^{-3})$, assuming parabolic density profile $n_i(r, z_0) = n_{max}\,(1 - r^2/r_p^2(z_0))$.

Table 1: Definitions and typical values of operating parameters for 24 kW VASIMR thruster.

Axial profiles for basic plasma parameters are shown in Figure 2. The Debye length l_D is much less than the plasma radius r_p everywhere, therefore the plasma quasi-neutrality will hold except in very localized sheath regions. Although collisional processes can play an important role in the plasma source region, the exhaust can be assumed reasonably collisionless beyond the central section as long as the mean free path l_{mfp} for various collision processes is much larger than plasma characteristic length. While the electrons follow the magnetic field through most of the region of interest, the ion Larmor radius r_L^i eventually becomes larger than the magnetic field curvature radius.

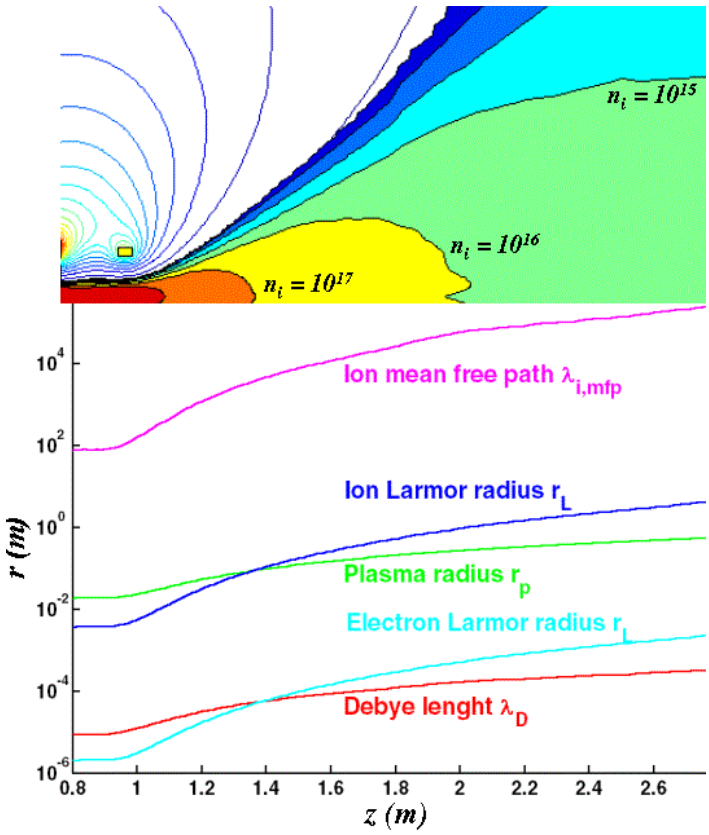

Figure 2: Plasma density profile (top) and scale lengths (bottom) of 24 kW VASIMR thruster.

ANALYTIC ESTIMATES FOR PLASMA DETACHMENT

A scaling analysis, also proposed by Dr. Roald Sagdeev (and reproduced below), is helpful in understanding some of the physics. In the VASIMR plasma exhaust, the magnetic flux is conserved. Thus, if B is the vacuum magnetic field and r_p is the radial coordinate plasma radius r_p, then

$$B \sim \frac{1}{r_p^2}.$$

From particle flux conservation, the plasma density n has the same dependence on r_p as B:

$$n \sim B \sim \frac{1}{r_p^2}.$$

Assuming that ion kinetic energy is a constant in the plasma exhaust (when the axial ambipolar electric field is neglected): $W \sim const$, the plasma beta, defined through the total energy W, has the following dependence on plasma radius:

$$b \sim \frac{nW}{B^2} \sim \frac{1}{B} \sim r_p^2.$$

This estimate shows that the ratio of plasma kinetic energy density to the magnetic field energy density increases downstream. When beta is greater than unity, the plasma has enough energy to stretch the magnetic field lines along the flow and thereby detach from the thruster. The condition $b > 1$ also means that the flow velocity is greater than the Alfvén velocity, which shows that plasma detachment is essentially a transition from sub-Alfvénic to super-Alfvénic flow. Similarly to what occurs in a supersonic flow created by the Laval nozzle, perturbations in the super-Alfvénic plume cannot be left in the sub-Alfvénic region and leave the system together with the outgoing flow. Our numerical simulations confirm this behavior.

PARTICLE TRAJECTORY SIMULATIONS OF THE PLASMA PLUME

The magnetic and electric fields, plasma density and electric current density are assumed at steady state and having cylindrical symmetry, which leaves dependence only on radial and axial coordinates r and z.

The magnetic field vector is a sum of the fields generated by the external coil and by the plasma current: $B(r, z) = \boldsymbol{B}_0(r, z) + \boldsymbol{B}_p(r, z)$. The electric field in the plasma plume is the ambipolar electric field: $\boldsymbol{E}(r,z) = \boldsymbol{E}_p(r, z)$.

The particle simulation currently incorporates five integrated models for calculation of these fields as shown in Figure 3.

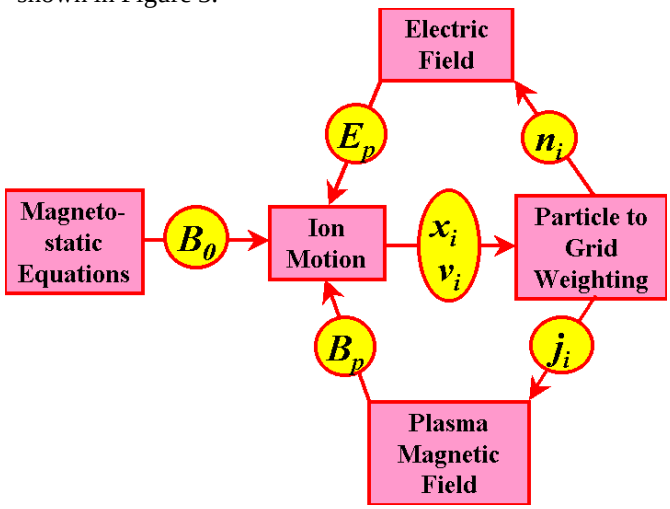

Figure 3: Mathematical simulation of plasma in VASIMR.

First, the magnetostatic field produced by the magnet coils, $\boldsymbol{B}_0(r, z)$, is accurately generated. This field does not change throughout the remaining calculation.

Second, a fully nonlinear particle model, that is currently collisionless, calculates the ion positions and velocities $\boldsymbol{x}_i(t)$, $\boldsymbol{v}_i(t)$ by solving the momentum equation.

The Lorentz force is calculated from the static and RF fields obtained from the Maxwell equation solvers in a three-dimensional space.

Third, the ion density, $n_i(r, z)$ and ion current density $\boldsymbol{j}_i(r, z)$ are calculated from the ion positions and velocities averaging over the gyro-motion, using a particle to grid weighting. The resulting ion density is approximately equal to the electron density in a quasineutral approximation, and it is fed into the fourth step.

The fourth step iterates over the previous models using $n_i(r, z)$ and a Boltzmann approximation for the electron distribution to solve Poison's equation for the steady state plasma potential giving $\boldsymbol{E}_p(r, z)$. This field further modifies the plasma density and hence the RF coupling.

The steady state plasma current density, $\boldsymbol{j}_i(r, z)$ becomes important in the exhaust region where $\boldsymbol{B}_p(r, z)$ can become significant compared with the fields from the magnet coils. Thus, the fifth and final step calculates steady state magnetic field corrections caused by the plasma in the exhaust region.

1) Magnetostatic Equations.

The magnetostatic problem is a steady-state case of two vector Maxwell equations:

$$\nabla \times \frac{1}{m} \boldsymbol{B}_0 = \boldsymbol{j}_0, \qquad \boldsymbol{B}_0 = \nabla \times \boldsymbol{A}_0, \tag{1}$$

where $\boldsymbol{B}_0$ is the vacuum magnetic induction vector, m is the magnetic permeability, $\boldsymbol{j}_0$ is the current density in electromagnets and $\boldsymbol{A}_0$ is the magnetic vector potential. When modeling the VASIMR system, the assumptions of cylindrical symmetry and constant magnetic permeability m are valid. In that case, the magnetic vector potential $\boldsymbol{A}_0$ (as well as current density vector $\boldsymbol{j}_0$), written in the cylindrical coordinate system (r, f, z), has only an azimuthal nonzero component: $\boldsymbol{A} = (0, A_f(r, z), 0)$ and the problem (1) can be rewritten in the following form:

$$-r \frac{\partial}{\partial r} \frac{1}{r} \frac{\partial F}{\partial r} - \frac{\partial^2 F}{\partial z^2} = m r j_0, \tag{2}$$

where $F(r, z) = r A_f(r, z)$ is the magnetic flux.

Equation (2) is solved with a high level of accuracy using a finite difference scheme, which is solved by a fast iterative method, described in previous publications[16, 17]. Figure 1 demonstrates the numerical solution for the vacuum magnetic field for a 24 kW VASIMR thruster. The calculated vacuum magnetic field $\boldsymbol{B}_0$ is used in both particle and MHD calculations.

2) Particle Dynamics.

The ion motion satisfies the following equation of motion:

$$m_i \frac{d\boldsymbol{v}_i}{dt} = e(\boldsymbol{v}_i \times \boldsymbol{B} + \boldsymbol{E}). \tag{3}$$

The single particle trajectories are integrated from equation (3) with an adaptive time-scheme, which can quickly solve extensive particle simulations for systems of hundreds of thousands of particles in a reasonable time (1-2 hours), and without the need for a powerful supercomputer. The particle calculation method is described in previous publications[18,19,20].

Figure 4 illustrates magnetic field lines and a typical ion trajectory in the exhaust area of the VASIMR. From the ion trajectory observation, one can see the beginning of the particle detachment from the magnetic field in the exhaust area with weak magnetic field.

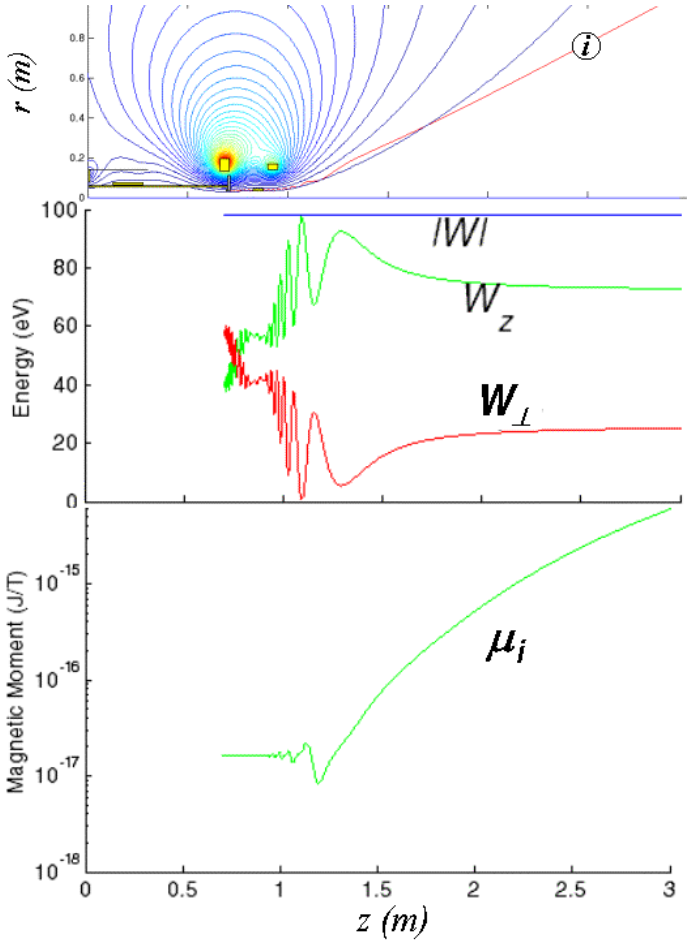

Figure 4. Top: Magnetic field lines and test ion trajectory in the VASIMR. Middle: Total, axial and perpendicular energies of the test ion. Bottom: Magnetic moment of the test ion trajectory. The ion detachment due to Larmor radius increase is observed.

The ion Larmor radius $r_L = m_i v_{i\wedge} / (q B)$ is rather small inside and near the thruster. However, it increases significantly down the flow, when the trajectory converges to a straight line. In the magnetic nozzle, the ion rotational energy converts into axial energy, which is demonstrated in the middle part of the Figure 4.

Since the magnetic flux $B r_p^2$ is a constant, where r_p is a plasma radius, the magnetic field goes down as fast as r_p^{-1}. The calculations show in the bottom of Figure 4, that the magnetic moment $m_i = m_i v_{i\wedge}^2 / (2 B)$ is approximately constant inside and near the thruster ($0.7 < z < 1.2$ *m*) but goes up in the exhaust area down the flow. It is accompanied with the perpendicular velocity $v_\perp$ going down as fast as r_p^{-1}. This makes the Larmor radius $r_L = 2 m_i / (q v_{i\wedge})$ increase faster than the magnetic moment.

During extensive particle simulation, one needs to define an initial ion velocity distribution. Current simulation assume a Maxwell distribution of ion velocity before going into the nozzle at $z = 0.7$ *m*. Figure 5 demonstrates initial ion velocity distributions inside the VASIMR engine at $z = 0.7$ *(B = 0.565 T)* and recalculated distribution at the boundary area with magnetic moment being conserved ($z = 1.2$ *m*, $B = 0.054$ *T).*

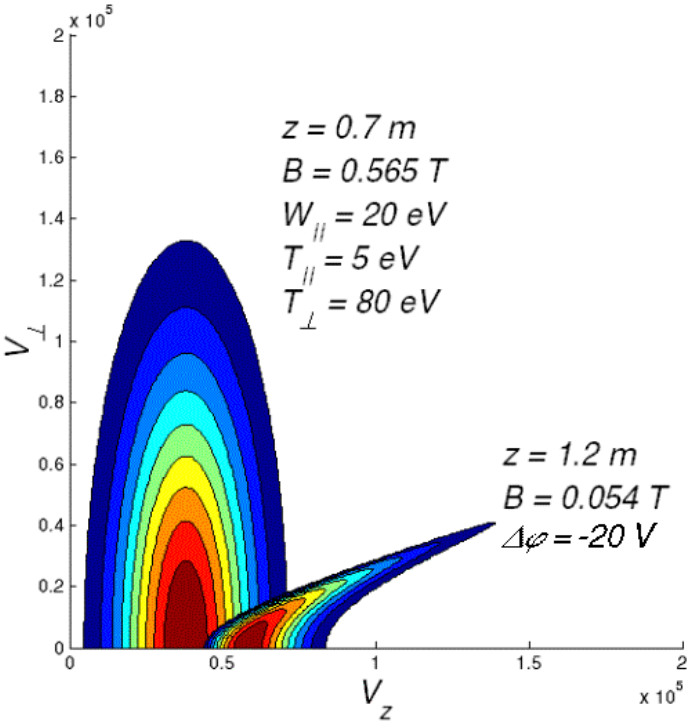

Figure 5: Initial ion velocity distributions at $z = 0.7$ *m*, $B = 0.565$ *T* and at $z = 1.2$ *m*, $B = 0.054$ *T.*

Note, that we moved the inlet position for the particles, from $z = 1$ *m (B = 0.265 T)* to $z = 0.7$ *m (B = 0.565 T).* This allows us to have à prefluid stabilization domain *0.3 m* long. In that stabilization domain the magnetic moment was conserved and initial conditions for particles where taken as $W_{||} = 20$ *eV*, $T_\wedge = 80$ *eV* at $z = 0.7$ *m*, to yield conditions $W_{||} = 50$ *eV*, $T_\wedge = 50$ *eV* at $z = 1$ *m.* This computational step gives a smoother calculated fluid variables of plasma density n, electric field E_p and magnetic field B_p for $z > 1$ *m.*

Figure 6 demonstrates the trajectory of a single electron with *5 eV* energy. In contrast to the ions, the complete electron attachment to the magnetic field is observed.

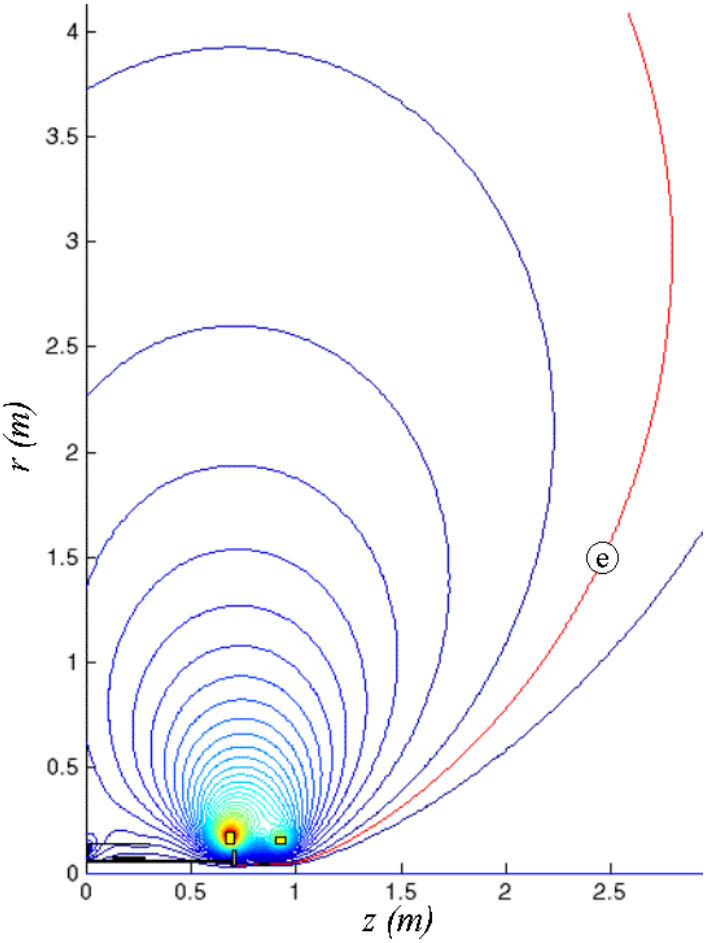

Figure 6: Magnetic field lines and test electron trajectory. The complete electron attachment is observed.

3) Particle to Grid Weighting

The ion density n_i is calculated by using a weighting method[5,10] for method of trajectories[9]. With a given distribution for the initial position and velocity vector, a large number (order of 10^5) of ion trajectories is

calculated. Every single trajectory is used to generate a number of particles distributed along it with equal time step between them. Plasma density clouds with a certain weight and a size of the finite difference cells are produced around each particle point, which after summation, became discrete ion density n_i defined constant at each finite difference cell, using the following formula

$$n_i(\boldsymbol{X}_j) = w_i \sum_k Q(\boldsymbol{X}_j - \boldsymbol{x}_k),$$

where $\boldsymbol{X}_j$ is a position of the j-cell, x_k is a position of k-particle, w_I is a particle weight, $Q(.)$ is a cloud density function. In our simulation, we used a continuous piece-wise-linear function with a support equal shape of the j-cell. The particle weight w_i is calculated, such that it makes the grid density equal given value at given point:

$$n_i(\boldsymbol{X}_0) = n_i^{\,0}.$$

The ion current density $\boldsymbol{j_i}$ is calculated by a technique, similar to that used to calculate the ion density in Figure 2. Namely,

$$\boldsymbol{j}_i(\boldsymbol{X}_j) = e w_i \sum_k Q(\boldsymbol{X}_j - \boldsymbol{x}_k)\boldsymbol{v}_k. \qquad (4)$$

4) Electrostatic Equations.

The electric field E_p can be calculated from the electric potential j:

$$\boldsymbol{E}_p = -\nabla j. \qquad (5)$$

In the system with cylindrical symmetry, it yields that $\boldsymbol{E}_p$ has only radial and axial nonzero components. The electric potential also satisfies the Poisson equation:

$$-\nabla^2 j = e(n_i - n_e), \qquad (6)$$

where the right-hand side is a plasma charge density. To avoid calculation of the electron density function, the Boltzmann relation is used:

$$n_e = n_0 \exp\left(\frac{ej}{kT_e}\right), \qquad (7)$$

where the bulk electron density n_0 is assumed equal the ion density at the plasma inlet (assuming that $j = 0$ there), and is a constant function along every magnetic field line.

In the present simulations the electron temperature T_e is assumed constant. Due to the very small value of the Debye length for the studied plasma system:

$$l_D = \sqrt{\frac{kT}{4\pi ne^2}} < 10^{-4}\, m, \qquad (8)$$

the Poisson equation (6) can be simplified to the quasineutrality relation: $n_i = n_e$, which gives the following formula for the electric potential:

$$j = \frac{kT_e}{e} \ln\left(\frac{n_i}{n_0}\right). \qquad (9)$$

To avoid $ln(0)$ calculations, the ion density can be adjusted by some small positive constant. Equation (9) has to be solved in the loop with particle simulations for the ions using an updated electric field. To achieve convergence in the self-consistent plasma – electric field calculations, under-relaxation (damping) is needed for updating the electric potential: $j_{new} = t j^{*} + (1-t) j_{new}$ with a relaxation parameter $t < 1$. In practical simulation, 10 iterations were enough to get a convergence with the relaxation parameter $t = 0.3$.

Figure 7 demonstrates the electric potential solution for the plasma system shown at Figure 2. The negative ambipolar electric potential in the exhaust area accelerates ions, which adds to the VASIMR performance.

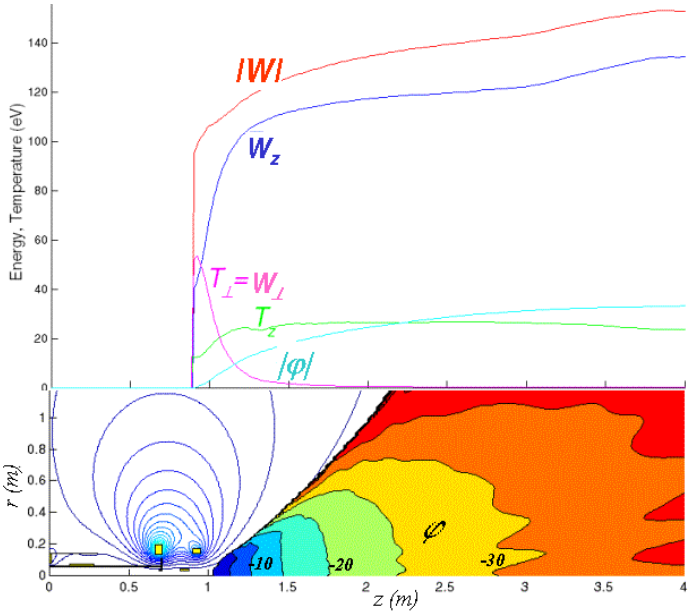

Figure 7. Top: Ion energy and temperature and electric potential in the 24 kW VASIMR thruster. Bottom: corresponding 2D contour-plot of the electric potential and magnetic field lines. The electric field is calculated self-consistently with the plasma density, shown in Figure 2.

5) Calculation of the internal plasma magnetic field

To calculate the plasma magnetic field, the plasma current has to be derived first. In an axisymmetric system with cylindrical symmetry, this current is purely azimuthal.

The momentum balance equation

$$r(\boldsymbol{u}\cdot\nabla)\boldsymbol{u} = \boldsymbol{j}_p \times \boldsymbol{B} \qquad (11)$$

yields the following dependence of plasma current due to the curvature of the vacuum magnetic field in the exhaust:

$$\boldsymbol{j}_p = \frac{r(\boldsymbol{u}\cdot\nabla)\boldsymbol{u}\times\boldsymbol{B}}{B^2}. \qquad (12)$$

The plasma current generates a plasma magnetic field that satisfies Ampere's law:

$$\nabla\times\frac{1}{m}B_p = \boldsymbol{j}_p. \qquad (13)$$

The ratio of the plasma magnetic field to the vacuum magnetic field can be estimated by the following expression:

$$\frac{B_p}{B} \approx \frac{mru^2 r_p}{B^2 a_p} = b\,\frac{r_p}{a_p}, \qquad (14)$$

where a_p is the magnetic field curvature. The particle simulation results are consistent with this analytical estimate.

The internal plasma magnetic field can be calculated using the same solver, as used for the vacuum magnetic field calculation. The only difference in this calculation is a current density source $\boldsymbol{j}_p$. The calculation of $\boldsymbol{B}_p$ should be iterated with the calculation of plasma velocity and density.

Figure 8 demonstrates the plasma current density due to the curvature of the magnetic field calculated by formula (12) and the magnetic field calculated by equation (13). In the plasma exhaust, the plasma magnetic field lines approach the direction of the z-axis.

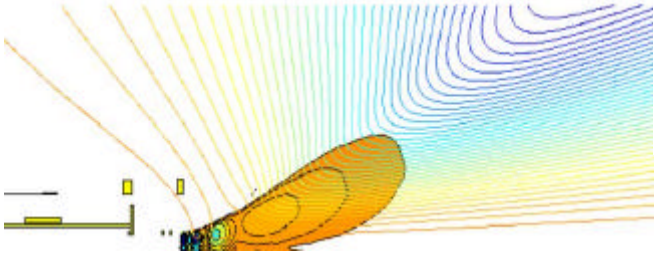

Figure 8: Curvature current density and corresponding magnetic field lines.

Note, that complete plasma current density calculated from particle trajectories by the formula (4) includes both magnetic field curvature and diamagnetic effects. The diamagnetic effect is essential only for high magnetic field in the area close to the thruster core and becomes negligible further away from it. It is demonstrated in Figure 9.

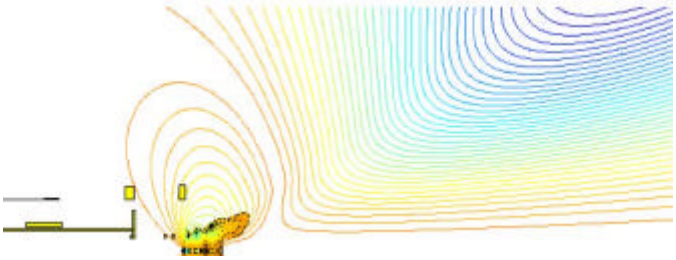

Figure 9: Plasma current density (diamagnetic and curvature) and corresponding magnetic field lines.

As numerical experiments show, the plasma-generated magnetic field in the area close to the thruster core is due to the diamagnetic effect and has an opposite direction to the vacuum magnetic field. In the exhaust area, when ions detach from the vacuum magnetic field, the plasma-generated field is due to the curvature current, which has the same direction. Although the value of beta reaches unity at $z = 3m$, the plasma-generated field is still smaller than the vacuum magnetic field for the studied range of parameters. That is shown in the Figure 10.

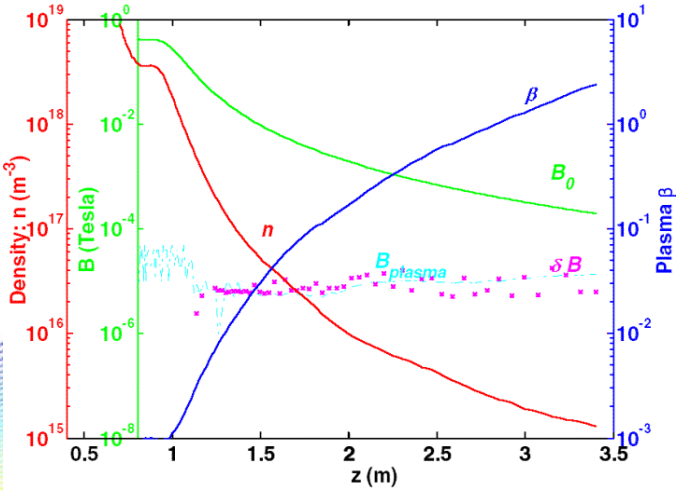

Figure 10: Demonstrating plasma detachment due to increasing plasma beta and plasma magnetic field approaching a constant. Plasma magnetic field B_p, calculated by the particle code is correlated well with semianalitical disturbed field *dB*, defined from the formula (14).

6) Observation of plasma detachment

During particle simulations we have observed the following indications of plasma detachment in VASIMR:

1) Axial ion energy W_z approaches a constant, which indicates that ion motion is not affected by the magnetic field, as shown in Figure 4. Thus, the velocity distribution function on the

axis becomes independent of *z* for large *z*. T example of the velocity distribution function demonstrated in Figure 11.

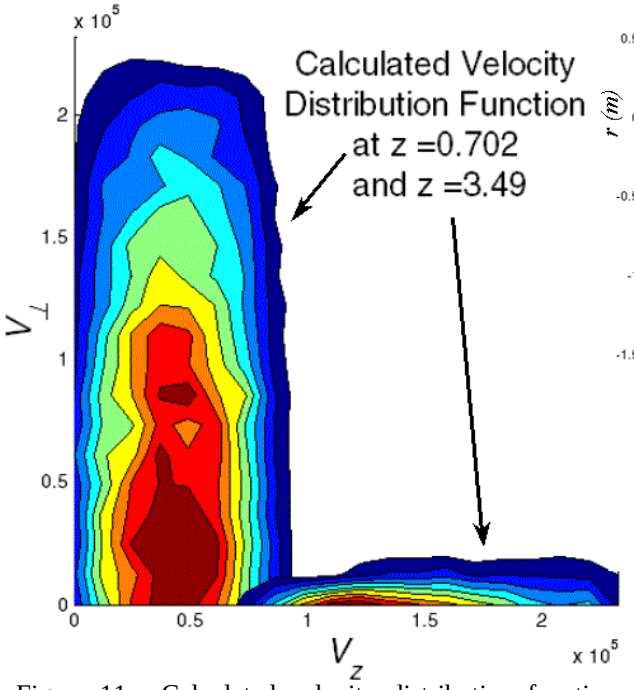

Figure 11: Calculated velocity distribution function using particle simulation. The effect of magnetic nozzle is observed.

2) Magnetic moment m_i increases (Figure 4).
3) Plasma b increases above 1. For the small power space-flight experiment VASIMR configuration, plasma b goes above one at the distance of *1.8* m from the nozzle magnet. Figures 10 and 12 demonstrate plasma b along axis *z* and in two-dimensional cross-section.
4) Plasma magnetic field is approaching a constant in the plasma exhaust (Figures 8, 9, 10). As demonstrated in Figure 10, the ratio of plasma magnetic field B_p to the vacuum magnetic field B_0 goes up from order *–4* at the nozzle magnet to order *–2* at 2 m from the nozzle magnet. Even in the area of plasma b larger than one, the plasma magnetic field is still much less than vacuum magnetic field. Also, Figure 10 demonstrates that plasma magnetic field B_p, calculated by the particle code correlates well with semianalitical disturbed field $dB = (r_p / a_p) B$, defined from the formula (14).
5) Ion Larmor radius r_L becomes greater than vacuum magnetic field line curvature a_p.

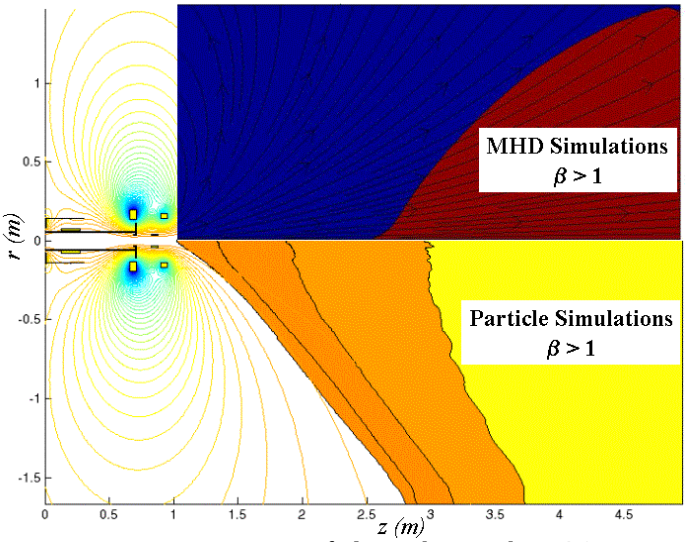

Figure 12: 2D picture of plasma beta in the VASIMR exhaust.

MHD SIMULATION WITH THE NIMROD CODE

A 3-D, MHD simulation tool is being developed and validated to bring the present theoretical analysis of the VASIMR nozzle/exhaust plasma region to a more accurate level. The simulation is able to reproduce quantitatively the exhaust plasma profiles at a distance from the engine where the detachment takes place.

The code is based on an upgraded version of *NIMROD*,[21] a code built for three-dimensional nonlinear fluid modeling of magnetized plasmas. This code is the result of a still ongoing multi-institutional effort supported by the U.S. Department of Energy and it is available in the public domain.

For this application, the *NIMROD* has been upgraded to introduce the density equation in the model (removing the incompressible fluid approximation of the current NIMROD release), and a provision for open-end boundary conditions and a plasma source term to simulate the exhaust flow. The applicable set of equations is:

1) Maxwell Equations

$$\frac{\partial \boldsymbol{B}_p}{\partial t} = -\nabla \times \boldsymbol{E} \ , \qquad \nabla \times \frac{1}{m} \boldsymbol{B}_p = \boldsymbol{j}_p$$

2) Continuity Equation

$$\frac{\partial r}{\partial t} = -\nabla \cdot r\boldsymbol{u}$$

3) Momentum Equation

$$r\left(\frac{\partial \boldsymbol{u}}{\partial t} + \boldsymbol{u} \cdot \nabla \boldsymbol{u}\right) = -\nabla \cdot (p\boldsymbol{I} + \boldsymbol{P}) + \boldsymbol{j} \times \boldsymbol{B}$$

4) Energy Equation

$$\frac{\partial p}{\partial t} + \boldsymbol{u}\cdot\nabla p = \frac{3}{2}\, p\nabla\cdot\boldsymbol{u} - \boldsymbol{P} : \tilde{N}\boldsymbol{u}$$

5) Ohm's Law (ideal MHD)

$$\boldsymbol{E} = -\boldsymbol{u}\times\boldsymbol{B}$$

The present simulations use the viscosity coefficient h to obtain a closure for the stress tensor as $\boldsymbol{P} = h\,\tilde{N}\boldsymbol{u}$.

Preliminary tests have been performed in a 2D *(r-z)* section of a cylindrical domain in 2D with the axis along the *z* direction. Open-end boundary conditions are imposed, along both the longitudinal and the radial direction. A plasma source term is injecting plasma in a low-density background environment and over time a plasma pulse is formed and starts to propagate along the magnetic nozzle. The simulation shows the initial transient of the pulse formation before the equilibrium between the exhaust rate and the injection rate is reached.

The results of the MHD codes are being used for validation of the particle code results and to obtain a better understanding of the plasma detachment. As shown in Figure 12, the results of particle simulation and MHD simulation on plasma beta analysis are very similar.

CONCLUSION

The described particle simulations in VASIMR demonstrate plasma detachment from the magnetic nozzle. Reasonable agreement between MHD and particle simulation is observed in plasma beta detachment analysis. The codes developed so far are being validated in the VX-10 laboratory experiment and assisting researchers in the design of a VASIMR flight demonstration experiment.

NOMENCLATURE

A	magnetic potential (Weber / m)
a_p	magnetic field curvature (m)
B	magnetic induction ($0 - 1$ Tesla)
E	electric field (Volt / m)
e	electron charge ($1.6\ 10^{-19}$ Coulomb)
F	thrust ($0.1 - 0.2$ N)
G	dimensionless detachment scaling parameter
g	gravitational acceleration (9.8 m / s^2)
I_{sp}	specific impulse ($5000 - 10^4$ s)
$\boldsymbol{I}$	identity tensor
$\boldsymbol{j}$	current density ($0 - 10^5$ Ampere / m^2)
k	Boltzmann constant ($1.38\ 10^{-23}$ J / K)
m	particle mass (D ion: $3.34\ 10^{-27}$ kg)
$\dot{m}$	propellant flow rate (10^{-6} kg / s)
n	plasma particle density ($0 - 2\ 10^{18}$ m^{-3})
P	power ($24{,}000$ Watt)
p	plasma pressure (Pa)
Q	particle cloud function
r, f, z	cylindrical coordinates: radial (m), azimuthal (rad) and axial (m)
r_L	Larmor radius ($10^{-2} - 1$ m)
r_p	plasma radius ($0.02 - 0.1$ m)
t	time (s)
T_e	electron temperature ($1 - 10$ eV)
T_i	ion temperature ($10 - 100$ eV)
u	exhaust (fluid) velocity (10^4 - 10^5 m / s)
v	particle velocity (ion: $10^4 - 10^5$ m / s)
W	energy (eV)
w	particle cloud weight
$\boldsymbol{X}$	cell position (m)
$\boldsymbol{x}_i$	ion 3-D position vector (m)
b	ratio of plasma kinetic pressure to the magnetic pressure ($0 - 10$)
h	viscosity (kg / (m s))
e	power efficiency (0.4)
F	magnetic flux (Tesla m^2)
j	electric potential (-100 - $+10$ Volt)
l_D	Debye length ($10^{-4} - 1$ m)
l_{mfp}	ion mean free path ($10^0 - 10^3$ m)
m	magnetic permeability ($1.25\ 10^{-6}$ Henry / m)
m_i	magnetic moment
$\boldsymbol{P}$	stress tensor
p	3.14159265358
r	plasma mass density ($0 - 7\ 10^{-9}$ kg / m^3)
t	relaxation parameter (0.3)

Subscripts:

0	vacuum, inlet
e	electron
i	ion
j	cell
k	particle
L	Larmor
p	plasma, proton
^	orthogonal to vacuum magnetic field $\boldsymbol{B}_0$
||	parallel to vacuum magnetic field $\boldsymbol{B}_0$

ACKNOWLEDGMENTS

This research was sponsored by NASA L. Johnson Space Center.

REFERENCES

1. Chang Díaz, F. R., "Research Status of The Variable Specific Impulse Magnetoplasma Rocket", *Proc. 39th Annual Meeting of the Division of Plasma Physics* (Pittsburgh, PA, 1997), *Bulletin of APS*, **42** (1997) 2057.

2. Chang Díaz, F. R., "Research Status of The Variable Specific Impulse Magnetoplasma

Rocket", *Proceedings of Open Systems' July 27-31, 1998*, Novosibirsk, Russia, American Nuclear Society, *Trans. of Fusion Technology*, **35** (1999) 87–93.

3. Chang Díaz, F. R., Squire, J. P., Ilin, A. V., et al. "The Development of the VASIMR Engine", *Proceedings of International Conference on Electromagnetics in Advanced Applications (ICEAA99), Sept. 13-17, 1999*, Torino, Italy, (1999) 99—102.

4. Chang Díaz, F. R., Squire, J. P., Bering, E. A. III, George, J. A., Ilin, A. V., Petro, A. J., and Cassady, L., "The VASIMR Engine Approach to Solar System Exploration", *Proceedings of 39th AIAA Aerospace Sciences Meeting and Exhibit' Jan. 8-11, 2001*, Reno, NV, AIAA 2001-0960 (2001) 11.

5. Birdsall, C. K., and Langdon, A. B., *Plasma Physics Via Computer Simulation*, Inst. of Physics Publishing, Bristol UK, (1995) 479.

6. Boyd, I. D., Keidar, M., and McKeon, W., "Modeling of a Plasma Thruster From Plasma Generation To Plume Far Field", *Proceedings of 35-th Joint Propulsion Conference, June 20-24, 1999*, Los Angeles, CA, AIAA-99-2300 (1999) 23.

7. VanGilder, D. B., Keidar, M., and Boyd, I. D., "Modeling Hall Thruster Plumes Using Particle Methods", *Proceedings of 35-th Joint Propulsion Conference, June 20-24, 1999*, Los Angeles, CA, AIAA-99-2294 (1999) 12.

8. Wang, J., Anderson, J., and Polk, J., "Three-Dimensional Particle Simulation of Ion Optics Plasma Flow", *Proceedings of 34-th Joint Propulsion Conference, July 13-15, 1998, Cleveland, OH*, AIAA-98-3799 (1998) 11.

9. Ilin, V. P., *Numerical Methods for Solving Problems in Electrophysics*, (in Russian) Nauka, Moscow (1985) 335.

10. Kosmahl, H. G., "Three-Dimensional Acceleration Through Axisymmetric Diverging Magnetic Fields Based on Dipole Moment Approximation," *NASA TN D-3782*, (1967) 28.

11. Sercel, J. C., "A Simple Model of Plasma Acceleration in a Magnetic Nozzle," *AIAA 90-2597*, (1990) 7.

12. York, T. M., Jacoby, B. A., and Mikellides, P., "Plasma Flow Processes Within Magnetic Nozzle Configuration", *J. of Propulsion and Power*, **8** (1992) 1023—1030.

13. Hooper, E. B., "Plasma Detachment from a Magnetic Nozzle," *J. of Propulsion and Power*, **9** (1993) 757—763.

14. Petro, A. J., Chang Díaz, F. R., Ilin, A. V., and Squire, J. P., "Development of a Space Station-Based Flight Experiment for the VASIMR Magneto-Plasma Rocket," *to be published in Proceedings of 40th AIAA Aerospace Sciences Meeting and Exhibit Jan. 14-17, 2002*, Reno, NV, AIAA 2002-0344 (2002).

15. Chang Díaz, F. R., Braden, E., Johnson, I., Hsu, M. M., and Yang, T. F., "Rapid Mars Transits With Exhaust-Modulated Plasma Propulsion", *NASA Technical Paper* 3539, Houston, TX (1995) 10.

16. Ilin, A. V., Chang Díaz, F. R., Gurieva, Y. L., and Il'in, V. P., "Accuracy Improvement in Magnetic Field Modeling for an Axisymmetric Electromagnet", *NASA Technical Paper 2000-210194*, Houston, TX (2000) 38.

17. Ilin, A. V., Bagheri, B., Scott, L. R., Briggs, J. M., and McCammon, J. A., "Parallelization of Poisson-Boltzmann and Brownian Dynamics calculation", *Parallel Computing in Computational Chemistry*, ACB Books, Washington D.C., (1995) 170—185.

18. Hockney, R. W., and Eastwood, J. W., *Computer Simulation Using Particles*, Inst. of Physics Publishing, Bristol UK, (1988).

19. Ilin, A. V., Chang Díaz, F. R., Squire, J. P., and Carter, M. D., "Monte Carlo Particle Dynamics in a Variable Specific Impulse Magnetoplasma Rocket", *Proceedings of Open Systems' July 27-31, 1998*, Novosibirsk, Russia, American Nuclear Society, *Trans. of Fusion Tech.* **35** (1999) 330—334.

20. Ilin, A. V., Chang Díaz, F. R., Squire, J. P., Breizman, B. N., and Carter, M. D., "Particle Simulations of Plasma Heating in VASIMR", *Proceedings of 36th AIAA/ASME/SAE/ASEE Joint Propulsion Conference' July 17-19, 2000*, Huntsville, AL, AIAA 2000-3753 (2000) 10.

21. Glasser, A. H., Sovinec, C. R., Nebel, R. A., Gianakon, T. A., Plimpton, S. J., Chu, M. S., Schnack, D. D., and the NIMROD Team, "The NIMROD Code: a New Approach to Numerical Plasma Physics," Plasma Phys. Control. Fusion **41**, A747 (1999).